Surface stoichiometry of pulsed ultraviolet laser treated polycrystalline CdTe

Brian J. Simonds,[1] Vasilios Palekis,[2] Brian Van Devener,[3] Christos Ferekides,[2] and Michael A. Scarpulla[1,4,a)]
[1]*Materials Science and Engineering Department, University of Utah, Salt Lake City, Utah 84112, USA*
[2]*Electrical Engineering Department, University of South Florida, Tampa, Florida 33620, USA*
[3]*University of Utah, Salt Lake City, Utah 84112, USA*
[4]*Electrical and Computer Engineering Department, University of Utah, Salt Lake City, Utah 84112, USA*

(Received 21 May 2014; accepted 24 June 2014; published online 3 July 2014)

The effects of nanosecond pulsed ultraviolet laser annealing on the surface stoichiometry of close-space sublimated polycrystalline thin films are investigated using angle-resolved x-ray photoemission spectroscopy (XPS). The raw data suggest the formation of a Cd-rich surface layer, but this is counter to the expectation based on Cd and Te vapor pressures above CdTe that predicts a Te-rich layer and to direct observation of elemental Te at the surface. In order to explain this apparent discrepancy, we analyze our XPS data in the context of prior reports of lateral segregation of Cd and Te at the surface after pulsed laser treatments with a simple model of angular dependent XPS in the presence of surface roughness. This analysis reveals that a uniform Te layer cannot explain our results. Instead, our analysis suggests that Te enrichment occurs near grain boundaries and that a sub-monolayer Cd layer exists elsewhere. These complex yet repeatable results underscore the challenges in measuring surface stoichiometry to high precision on films relevant for polycrystalline CdTe devices. It also suggests that the Cd and Te vapor pressures above grain boundaries may differ from those above grain interiors and that ohmic contact may be made preferentially at the grain boundaries after pulsed laser annealing. © *2014 AIP Publishing LLC*.
[http://dx.doi.org/10.1063/1.4887079]

I. INTRODUCTION

Ultraviolet (UV) pulsed laser annealing (PLA) of CdTe is a promising means to affect composition within a very shallow near surface region. The characteristic depth of the heat-affected region is the larger of $\sqrt{2D\tau}$ or the optical penetration depth, where D is the thermal diffusivity and τ is the laser pulse duration.[1] For a 25 ns, 248 nm laser pulse incident to CdTe the penetration depth is ≈10 nm. The thermal diffusion length is ≈500 nm. However, thermally activated kinetics (i.e., diffusion and evaporation) will be significant only near the surface because of the extremely-high transient temperature gradients.[2] Therefore, nanosecond UV PLA will primarily affect the free surface of CdTe, which forms the back contact for superstrate CdTe photovoltaic devices while minimally impacting the bulk of the film. We recently demonstrated the use of PLA as a dry process for ohmic contact formation for photovoltaic devices[3] and it has also been used in forming CdTe radiation detectors.[4–7]

When laser pulses of sufficient energy density are incident to a crystalline CdTe (c-CdTe) surface, it has been shown that a Te-rich surface is formed. Evidence of this was first presented by Brewer *et al.*[8] using Auger electron spectroscopy and has since been corroborated by several others.[3,9–12] The Te-enrichment is created by exploiting the large difference between Cd and Te vapor pressures over CdTe that occurs at high temperatures.[8,11] With the application of an appropriate UV laser pulse, temperatures approaching but not exceeding the melting temperature can be reached causing preferential evaporation of Cd from the surface.[13] The first experiment to apply UV PLA to polycrystalline CdTe (p-CdTe) was by Nelson *et al.* who showed that Te-agglomeration occurs largely at the grain boundaries (GB) from high resolution x-ray photoelectron microscopy that necessitated a synchrotron radiation source.[12] Interestingly, this work also found that a slight Cd enrichment occurred at the surfaces of the grain interiors, even though the overall effect of PLA was a Te enrichment at the surface. The unirradiated films showed a similar but much lower contrast spatial distribution of surface Cd and Te. Additionally, they used highly idealized, low surface roughness p-CdTe samples that were grown, laser treated, and measured all without breaking ultrahigh vacuum (UHV). Our work shows how segregation of this type can affect, as well as be inferred from, laboratory-scale XPS analysis on practical device-ready p-CdTe.

Here, we explore the surface stoichiometry of PLA treated p-CdTe with XPS. The raw data suggest that overall the PLA makes the surface Cd-rich as opposed to Te-rich. At first, this result appears to contradict our earlier observations of elemental Te at the surface and improved ohmic contacts following PLA.[3] To understand this apparent discrepancy, we calculated the XPS-indicated stoichiometry using a model that incorporates the Te and Cd segregation observed by Nelson *et al.* along with features of a rough surface indicative to p-CdTe. The analysis shows that the stoichiometry of p-CdTe taken from XPS is highly sensitive to segregation

a)Author to whom correspondence should be addressed. Email: scarpulla@eng.utah.edu

at the surface even if these overlayers only have sub-monolayer thicknesses. The results in this article underscore the importance of considering this effect for XPS analysis of stoichiometry at CdTe surfaces.

II. METHODS

A. Experimental

The films used for this study were prepared by close-space sublimation of CdTe onto alumina substrates, which is described elsewhere.[14] These films were about 5 μm in thickness and are typical of those used in high quality photovoltaic devices. Scanning electron microscopy micrographs were obtained using a field emission FEI Quanta 600 with a field emission gun system. Optical profilometry data were taken on a Zygo NewView system with a 20× objective lens. Surface roughness modification was achieved through low-angle ion-mill etching using a Fischione Instruments 1060 SEM Mill in an Ar-filled chamber. The dual ion sources were set to 5 keV at a 1° angle to the sample surface and etched for 25 min. Laser annealing was accomplished using a KrF excimer laser operating at 248 nm with 25 ns pulses at either 55 or 65 mJ/cm^2. Multiple pulse treatments were performed at a 10 Hz repetition rate, which gave long enough time for heat to dissipate between pulses.

XPS experiments were carried out on a Kratos Axis Ultra DLD system using a monochromatic Al x-ray source. Both high and low resolution scans were performed with pass energies of 40 eV and 160 eV, respectively. In order to mitigate the effects of surface oxides and adventitious carbon on the XPS results, the following procedure was developed. First, the as-deposited sample was placed in the UHV XPS analysis chamber where a 4 keV Ar-ion sputter etch was applied until neither C nor O was visible in a broad energy, low resolution scan. This etch was performed at normal incidence to the film surface for ≈60 s and is not to be confused with the low-angle ion-mill etch described for surface roughness modification. After removing signs of C and O, the Cd and Te atomic concentrations were quantified and used as the pre-anneal reference. Next, the sample was moved from the analysis chamber, via an inert atmosphere transfer device, to an argon gas purged glove bag where it was placed in the gas-tight laser annealing chamber. This was to ensure that the sample did not come into contact with ambient air and develop surface oxides. Following laser treatment in the Ar-filled chamber, the sample was returned to the XPS analysis chamber by reversing the process. The Ar-ion sputtering was achieved by rastering over a 3×3 mm^2 area whereas the spot size of the XPS measurement was $300 \times 700\ \mu$m^2. Fiduciary marks were used to ensure that the measured spot was well within the sputtered area before and after laser annealing so that etch crater side wall issues were not encountered. Analysis of XPS spectra was carried out using CasaXPS analysis software. XPS quantification was achieved by analyzing the high resolution spectra taken with 0.1 eV step sizes. A pseudo Voigt function of 30% Gaussian character to 70% Lorentzian character was used to fit these data after a Shirley background subtraction.

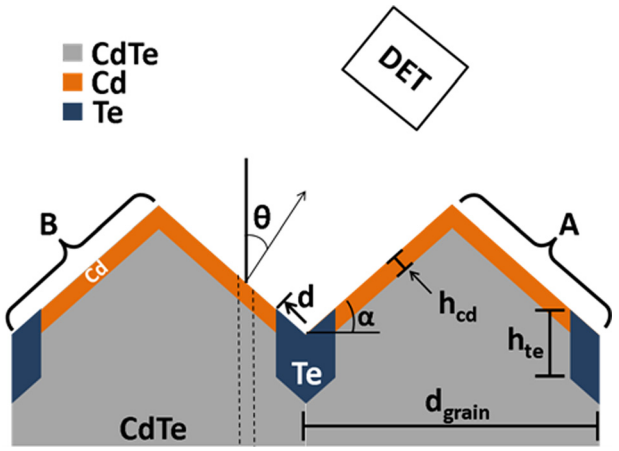

FIG. 1. Diagram of the model used in the study with the detector (DET) above the film surface. See text for details and definitions.

B. Computational model

We developed a greatly simplified 2D geometric model for the complex surface conditions that exist for p-CdTe. The surface is assumed to be an array of triangular prisms creating parallel ridges as seen in Fig. 1. Similar models have been used by others to incorporate surface morphology effects on XPS signal intensities.[15–17] In 2-dimensions, the model profile seems reasonable when compared to the surface roughness cross sections (see Figs. 2(b) and 2(c)), but in 3-dimensions, this is clearly not true. The model used here was chosen as it incorporates the salient features of our material (faceted topology) and can readily incorporate the anticipated spatial segregation: Te enrichment at GB with Cd enrichment elsewhere.[12] Therefore, this model should be effective at predicting the qualitative behaviors seen in our measurements. Modeling techniques have been developed for dealing with more complex geometries,[18] including randomly corrugated surfaces.[19–22] However, these do not readily allow for spatial segregation of multiple overlayers as is necessary for our current investigation.

A diagram of our model is shown in Fig. 1. Surface inhomogeneities are approximated by elemental Cd and Te overlayers with Te near the GBs and Cd elsewhere. Abrupt transitions between the Te-rich and Cd-rich regions are assumed. The regions between successive valleys represent one grain with GBs extending downward from the valleys. The thicknesses of the Cd and Te layers, parameterized by h_{cd} and h_{te}, respectively, are exaggerated in Fig. 1 as they are on the order of single nanometers or less. The extent to which the Te-rich layer extends outward from the GBs is given by the parameter d. The grain width is d_{grain} and the surface roughness is parameterized by the angle α that the peak's slope makes with a planar surface. The trajectory of a photoemitted electron is described by the angle θ between the global surface normal and the ray to the detector (labeled "DET" in Fig. 1). By defining θ thusly, we are assuming that all electrons travel in straight lines, without scattering, towards the detector. From this diagram, it is seen that due to surface topography even at $\theta = 0$, one is essentially performing angle resolved XPS on an electron photoemitted from

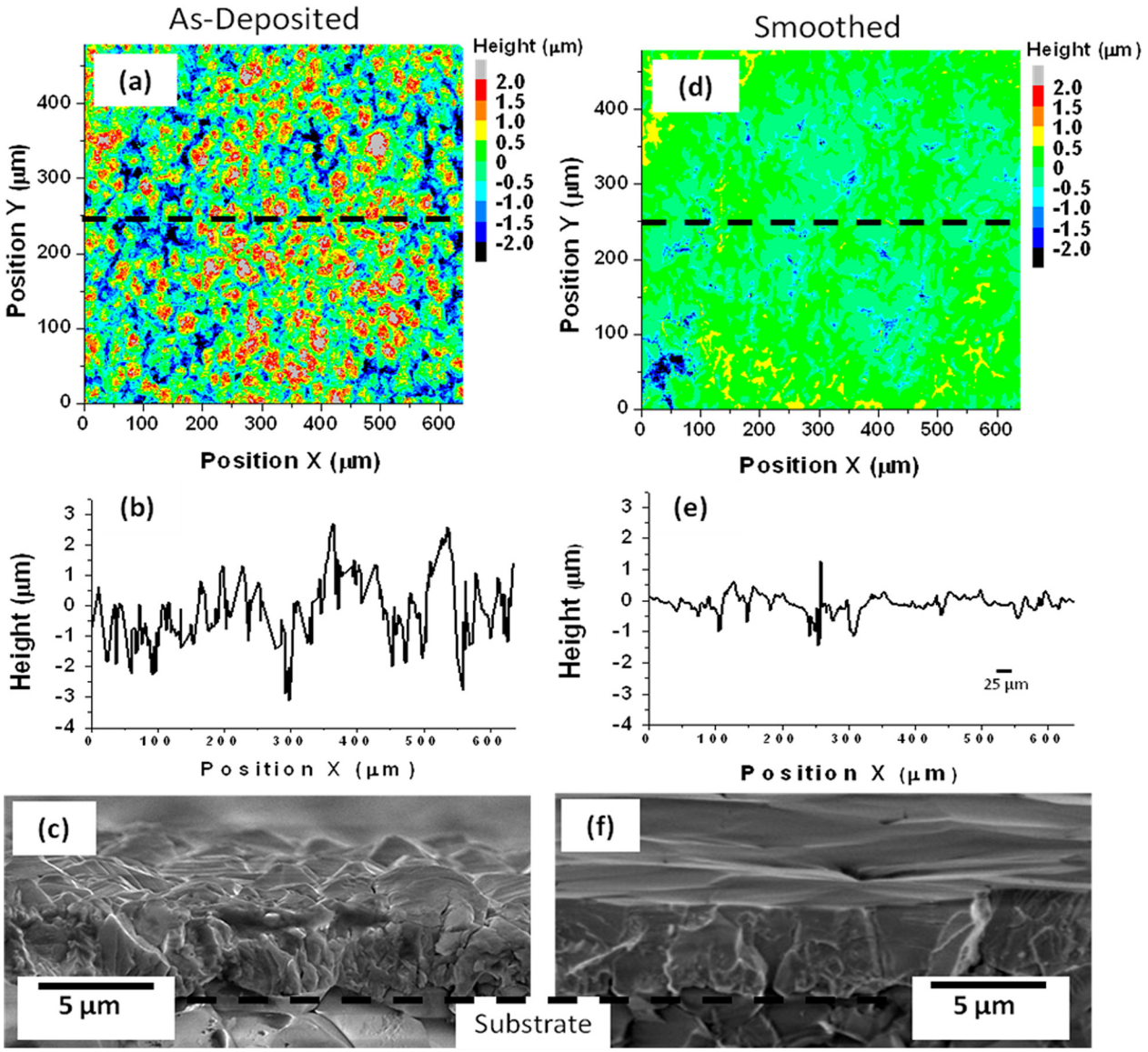

FIG. 2. Topographic data from optical profilometry showing surface roughness of the as-deposited (a) and ion-mill smoothed (d) films. Plots (b) and (e) show cross sectional data along the dashed lines in (a) and (d) for the as-deposited and smoothed samples, respectively. Cross-sectional SEM micrographs of both films are shown in (c) and (f) with the substrate CdTe interface marked with the dashed line. A comparison of the approximate scale of the SEM micrographs is given by the 25 μm bar in (e).

any point on the surface. Two types of facets are considered: those that increasingly face the detector (A) and those that increasingly face away from the detector as θ increases from 0 (B). It is also assumed that x-ray shadowing is not significant as the x-ray penetration depth is about an order of magnitude larger than even the roughest sample studied here.[22]

The molar fractional F_x of a constituent atom x in a material as determined from XPS raw data is given by[23]

$$F_x = \frac{I_x}{I_x^{\infty}}, \tag{1}$$

where I_x^{∞} is an atomic sensitivity factor. In our model, the total intensity I_x of each constituent (Cd or Te) is calculated by dividing the surfaces of A and B into i segments and determining the intensities for each segment. These are then summed to give a total intensity for Cd and Te. Each segment's contribution to the total XPS intensity, $I_{i,j,k}^{A/B}$, is calculated as

$$I_{i,1,k}^{A/B} = Cf_{j,k}\int_0^{h_k} n_{i,1,k}\exp\left(\frac{-z}{\lambda_i\cos(\theta\pm\alpha)}\right)dz = Cf_{j,k}\,\lambda_i\,n_{i,1,k}\cos(\theta\pm\alpha)\left[1-\exp\left(\frac{-h_k}{\lambda_i\cos(\theta\pm\alpha)}\right)\right], \tag{2}$$

$$I_{i,2,k}^{A/B} = Cf_{j,k}\int_{h_k}^{\infty} n_{CdTe}\exp\left(\frac{-z}{\lambda_i\cos(\theta\pm\alpha)}\right)dz = Cf_{j,k}\,\lambda_i\,n_{CdTe}\cos(\theta\pm\alpha)\exp\left(\frac{-h_k}{\lambda_i\cos(\theta\pm\alpha)}\right). \tag{3}$$

Equations (2) and (3) extend from analyses derived for inhomogeneous solids with buried surface layers on flat surfaces.[16,22,24] Here, we have included lateral composition variations as well. The superscript for the A or B facets determines either addition or subtraction in the argument of the cosine function, respectively. Equation (2), where $j=1$, gives the contribution from the overlayer. When $k=1$, the Te layer is designated and when $k=2$ the Cd layer. Equation (3) is the contribution to the total intensity from the subsurface CdTe ($j=2$), which is assumed to be stoichiometric. Therefore, the value of k determines the integration limit with $h_1=h_{Te}$ and $h_2=h_{Cd}$. Similarly, the atomic density, $n_{i,j,k}$, is equal to n_{Te} for $j=k=1$, n_{Cd} for $j=1$ and $k=2$ and n_{CdTe} for $j=2$ and $k=1,2$. The parameter $f_{j,k}$ is the atomic fraction of the analyzed element (either Cd or Te) and is 1 for (j,k) values of (1,1) or (1,2) and 0.5 for (j,k) values of (2,1) or (2,2). The constant C contains all instrument related functions, which are assumed to be the same whether measuring Cd or Te, and is therefore cancelled out in the final calculation of the Cd:Te ratio. The electron attenuation length is given by λ_i and is assumed to be 1.5 nm for all layers in the film.[25] The values of all constants used are listed in Table I.

To find the total XPS intensity, the contributions from every segment are summed over the total number of segments, i_{max}.

$$I_{j,k}^{A/B}=\frac{I_{i,j,k}^{A/B}}{i_{max}}\sum_{i=1}^{i_{max}}\delta_{i,j,k}^{A/B}(\theta). \tag{4}$$

The parameter, $\delta_{i,j,k}^{A/B}$, is determined by the position of the ith segment. For every segment, there exists a critical angle, θ_i^{cr}, such that when $\theta>\theta_i^{cr}$, the contribution of that segment's photoelectrons to the total XPS intensity is blocked by the opposing grain facet, which describes the well-known shadowing effect caused by surface roughness. For facet A, θ_i^{cr} is found by dividing the vertical distance to the opposing peak by the lateral distance to this peak and taking the inverse tangent.[15] For facet B, all i segments have the same critical angle determined by α. These conditions are expressed as

$$\delta_{i,j,k}^{A}=\begin{cases}0;\ \theta\geq\theta_i^{cr}\\ 1;\ \theta<\theta_i^{cr},\end{cases} \tag{5}$$

$$\delta_{i,j,k}^{B}=\begin{cases}0;\ \theta\geq 90-\alpha\\ 1;\ \theta<90-\alpha.\end{cases} \tag{6}$$

Contributions to the XPS intensity are aggregated into those that result in a Cd signal and those that contribute to the Te signal

$$I_{Cd}=\sigma_{Cd}(I_{1,2}^{A}+I_{1,2}^{B}+I_{2,1}^{A}+I_{2,2}^{A}+I_{2,1}^{B}+I_{2,2}^{B}), \tag{7}$$

$$I_{Te}=\sigma_{Te}(I_{1,1}^{A}+I_{1,1}^{B}+I_{2,1}^{A}+I_{2,2}^{A}+I_{2,1}^{B}+I_{2,2}^{B}). \tag{8}$$

These terms are weighted by the photoelectron cross sections (σ) of each atom type. The final step in calculating Cd:Te is to divide Eqs. (7) and (8) by one another as well as their sensitivity factors as described in Eq. (1).

TABLE I. The constants used for model calculations.

Constant	Value
λ_i	1.5 nm
d_{grain}	1 μm
$n_{i,1,1}=n_{Te}$	2.94×10^{22} atoms/cm^3
$n_{i,1,2}=n_{Cd}$	4.63×10^{22} atoms/cm^3
$n_{i,2,1}=n_{i,2,2}=n_{CdTe}$	1.47×10^{22} atoms/cm^3
$\alpha_{as\ deposited}$	10.4°
$\alpha_{smoothed}$	3.2°
I_{Cd}^{∞} [a]	3.5
I_{Te}^{∞} [a]	5.4
σ_{Cd} [b]	11.95
σ_{Te} [b]	18.06

[a]Ref. 26.
[b]Ref. 27.

III. RESULTS AND ANALYSIS

The topography of a sample analyzed by XPS can greatly affect the measured results. We have investigated the surface roughness of our films by optical profilometry and electron microscopy, which is summarized in Fig. 2. Figs. 2(a) and 2(d) show 2D optical profilometry data of an as-deposited and smoothed film, respectively. The calculated surface roughness of the as-deposited film is 1.0 μm root-mean squared (RMS) that reduced to 350 nm in the smoothed film. Figs. 2(b) and 2(e) give a line scan taken along the dashed lines in Figs. 2(a) and 2(d), respectively. Figs. 2(d) and 2(e) are plotted on the same scale as Figs. 2(a) and 2(b), respectively, to help visualize this decrease in RMS. It is noted that even in the smoothed sample, the RMS is still very large as compared to the electron escape depth that dictates the depth scale of XPS measurements. In addition, although the surface roughness was reduced by about a factor of three, the same qualitative features of valleys and hillocks are found in Fig. 2(b) as in Fig. 2(e) meaning our model should apply equally well to both. Also, we point out that it is the relative coverage of the Te and Cd rich regions that matters and not the absolute grain size. Figs. 2(c) and 2(f) show cross-sectional SEM micrographs of both the as-deposited and smoothed film surfaces, which corroborate the findings of the optical profilometry.

The surface roughness is parameterized in the model by a single angle, α. This angle was experimentally determined from the profile data in Fig. 2. By integrating the derivative of the profile data from Figs. 2(b) and 2(e), one can define an average slope, S_{avg}, as[22]

$$S_{avg}=\frac{1}{L}\int_0^L\left|\frac{\partial z}{\partial x}\right|dx,$$

where L is the total width of the profile scan, z is the height, and x is the lateral position. From this, it is possible to calculate an average value of α from

$$\alpha_{avg}=\tan^{-1}(S_{avg}).$$

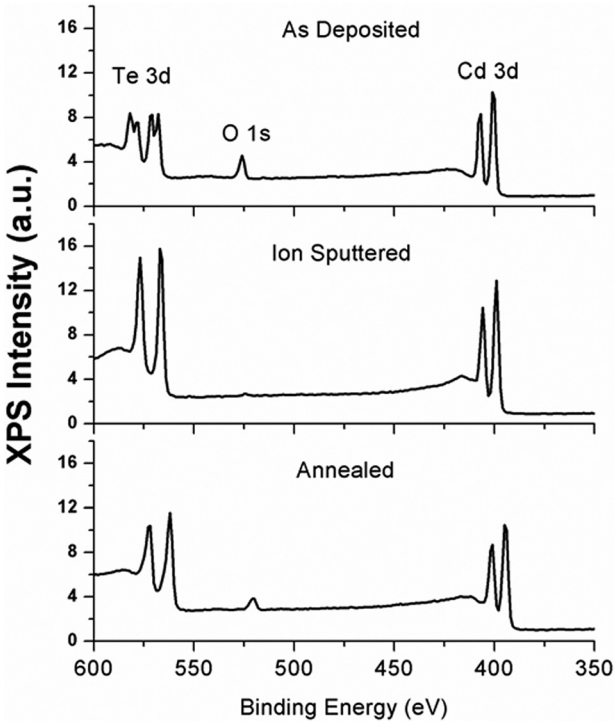

FIG. 3. XPS data showing the sequence of measurement starting with the top showing the as-deposited film. The middle data follow ion sputtering to remove surface oxides and the bottom is following UV laser treatment.

This was calculated for about 20 horizontal scans in each topographic map and averaged. For the as-deposited sample, $\alpha = 10.4°$; and for the ion-milled sample, $\alpha = 3.2°$.

Fig. 3 shows a series of XPS spectra of films taken at different steps of the XPS analysis procedure described in the experimental section. An oxygen 1s signal appears in the as-deposited material. Oxygen is in the form of Te oxide and Cd oxide as evidenced by two pairs of doublets for both Te and Cd 3d peaks[28] in the top graph. The lower binding energy doublet of the Te 3d peaks at 568 eV and 578 eV are from Te bonded to Cd whereas the higher one at 571 eV and 582 eV are from Te oxide.[29] The Cd oxide doublet is more difficult to distinguish as they lie closer in binding energy to the doublet from Cd bonded to Te.[28] However, a narrowing of the Cd 3d peaks seen following Ar-ion sputtering betrays their presence, which was also confirmed by high resolution scans. Fig. 3 shows that within the sensitivity of these XPS scans, the presence of oxygen disappears after Ar-ion etching, thus confirming its origin as being from a surface oxide layer. However, after laser annealing, a small O 1s signal reappears. Because of the precautions of the inert atmosphere transfer and knowledge of the CdTe deposition, it is suspected that this signal arises from oxygen incorporated during CdTe CSS growth that was driven to the surface and reacted during laser annealing.

In order to quantify the stoichiometry of the surface, high resolution scans were performed with a spot size of $300 \times 700\ \mu m^2$. The measured pre-annealed value of the Cd:Te ratio (taken following Ar-ion sputter cleaning) at $\theta = 0°$ was found to be 1.30. A Cd-rich as-deposited surface is consistent with several results of XPS measurements from literature.[30,31] Following laser treatment at 65 mJ/cm^2 for 600 pulses, the measured Cd:Te ratio was 59.5:40.5 or 1.47. Therefore, it appears that the surface of the CdTe became more Cd enriched during the laser annealing process by about $13\% \pm 3\%$. This is counter to what is expected based on other experimental evidence[3,8–12,32–36] and predictions of thermodynamic modeling.[3,13] In light of the overwhelming evidence from several different groups and techniques, we believe that the calculated Cd enrichment given by XPS is a result of the Te enrichment being masked by a very thin (sub-monolayer) Cd layer at the surface.

In order to test the effects of the surface morphology on our results, the RMS roughness was reduced by a low-angle ion-mill etching procedure that produced a film with approximately 3 times lower RMS. The same procedure for measuring XPS spectra on a pre- and post-annealed sample was followed. This sample was laser treated for 60 s at 10 Hz with a fluence of 55 mJ/cm^2. The Cd:Te ratio for the pre-laser treated sample was 1.16 that then increased to 1.28 for the laser treated sample. The smoothed sample shows an apparent increase of $10\% \pm 3\%$ following pulsed laser annealing. The fact that the smoothed and rough samples gives the same relative change in Cd:Te ratio due to PLA suggests that the surface roughness is not the main culprit skewing the Cd:Te results.

Fig. 4 shows model calculations of Cd:Te for various amounts of Cd and Te segregation at the surface. Fig. 4(a) plots the calculated Cd:Te ratio versus d, the distance that the Te region extends from a GB, when $\theta = 0°$ and $\alpha = 10.4°$ (the measured as-deposited value) where the thicknesses of the Cd and Te layers are equal in each curve. The circles (red) are for $h_{cd} = h_{te} = 0$ and as expected, Cd:Te approximately equals 1 and is independent of d, even for a non-smooth film. The small deviation from stoichiometry (~2%) in the non-overlayer material can easily be explained by uncertainties in the photoelectron cross sections and sensitivity factors used.[23] The triangles (blue) are for $h_{cd} = h_{te} = 0.5$ Å and the squares (green) for $h_{cd} = h_{te} = 2$ Å. To put these overlayer thicknesses into perspective, the atomic spacing of both elemental Cd and Te are approximately 3 Å (Ref. 37) so both of these overlayers are sub-monolayer. As seen from these curves, even this very small amount of elemental Cd and Te causes the overall XPS Cd:Te ratio to deviate strongly from stoichiometry. In fact, one sees that in the presence of such thin overlayers, how unlikely it is that XPS measurements will appear stoichiometric even though the near-surface bulk is perfectly stoichiometric. The measurements of Nelson *et al.*[12] showed that some amount of surface segregation existed in their as-deposited p-CdTe. If this is generally true, large deviations from stoichiometry from XPS should be expected and is one possible explanation for the large deviations reported in the literature. Similar curves were obtained for $\alpha = 3.2°$, and it was found that there was negligible difference in these curves as α was varied over a range of 0° to 20°. This suggests that the differences in surface roughness studied here are not large enough to drastically alter the measured Cd:Te ratio. This coincides with our experimental findings above.

The anticipated effect of laser annealing is simulated in Fig. 4(b) by assuming that the Te overlayer grows with

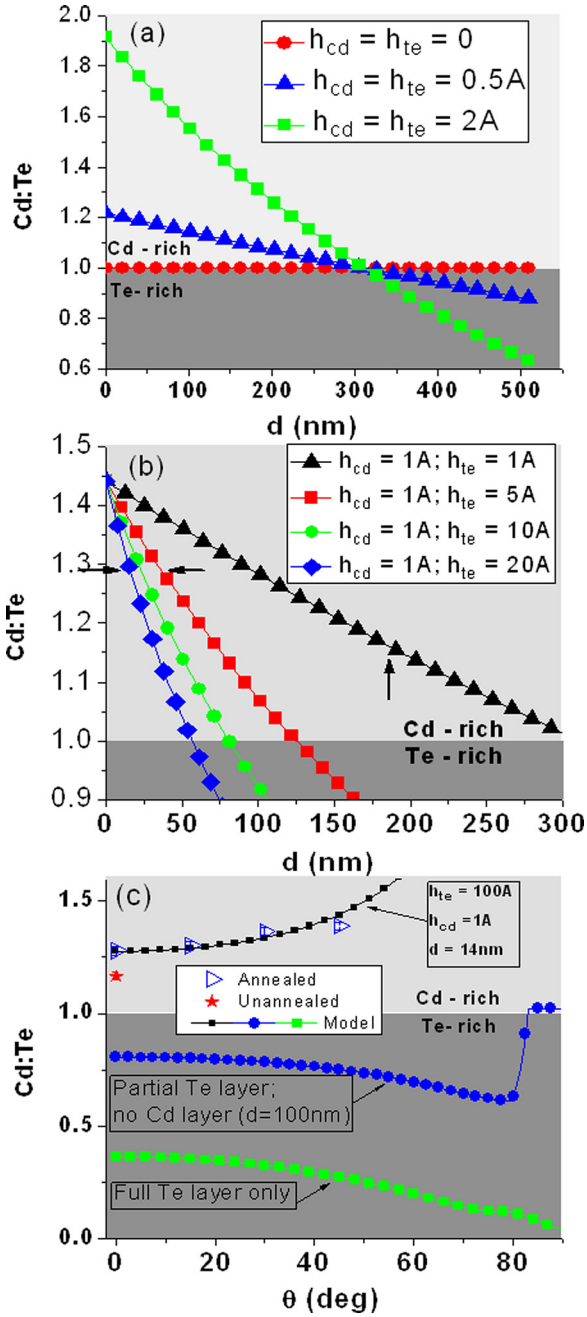

FIG. 4. Model calculations for various experimental situations. (a) $\theta = 0°$ where $h_{cd} = h_{te} = 0$ Å (circles, red), $h_{cd} = h_{te} = 0.5$ Å (triangles, blue), and $h_{cd} = h_{te} = 2$ Å (squares, green). (b) $\theta = 0°$ and h_{cd} constant at 1 Å with $h_{te} = 1$ Å (triangles, black), $h_{te} = 5$ Å (squares, red), $h_{te} = 10$ Å (circles, green), and $h_{te} = 20$ Å (diamonds, blue). (c) Angle-dependent calculations and data. The squares (green) assumes a uniform overlayer of Te ($h_{te} = 5$ Å). The circles (red) have only a partial Te overlayer with d = 100 nm and $h_{te} = 5$ Å. The open triangles (blue) are from angle-resolve XPS data after annealing with the pre-annealing stage given by the star (red). The solid triangle line running through these points were calculated with $h_{cd} = 10$ nm, $h_{te} = 1$ Å, and d = 14 nm.

respect to the Cd overlayer. The triangles (black) assume equal thicknesses of Cd and Te overlayers ($h_{Cd} = h_{Te} = 1$ Å) as a possible pre-anneal situation. As an example, the vertical arrow points to our measured pre-annealed value of Cd:Te. The other curves (red squares, green circles, and blue diamonds) increase the Te layer thickness to $h_{Te} = 5$ Å, 10 Å, and 20 Å, respectively, while the Cd overlayer is held constant at $h_{Cd} = 1$ Å. The horizontal arrows are at our measured value of Cd:Te following laser annealing. Qualitatively, these calculations suggest that our data can be explained if the laser induced Te enrichment is confined to a region very near GBs following laser annealing.

Calculations of angle-resolved XPS measurements are presented in Fig. 4(c) in addition to our measured data. The bottom curve (green squares) is for a uniform overlayer of Te 5 Å thick. The middle curve (blue circles) is for a partial Te overlayer (d = 100 nm and $h_{Te} = 5$ Å) and no Cd overlayer ($h_{Cd} = 0$). In both cases, the Cd:Te ratio moves more towards a Te-rich value as θ is increased from 0°. This is the opposite trend seen in our data. The feature near 80° is evidence of the well-known shadowing effect that occurs at $\theta = 90° - \alpha$.[15] Since this is much greater than the range of θ available to us experimentally, shadowing is not the cause of our Cd:Te ratio discrepancy. The top curve (black squares) is for $h_{Te} = 10$ nm and $h_{Cd} = 1$ Å and d = 14 nm. The inclusion of roughly a third of a monolayer of Cd causes the Cd:Te ratio to increase with θ, matching the experimental observation. The source of this rise is the surface sensitivity of XPS and the large surface area of the Cd overlayer relative to the Te overlayer. This can be seen when looking at the calculated Cd and Te intensities alone (Eqs. (7) and (8)). The Cd intensity remains relatively constant until θ reaches very large angles. However, for the thicker Te layers, there is an immediate reduction in Te signal with increasing θ. This can be seen in equation (2) as the angle-dependent argument of the exponential term is weighted by the overlayer thickness meaning thinner layers lead to a smaller angle dependence.

IV. DISCUSSION

Our calculations show that the trends in the experimental data can be replicated when Te is localized at GBs and a thin Cd overlayer is included elsewhere. It is possible to simulate the qualitative behavior of our data by only including a Cd overlayer. However, the presence of some surface region of Te enrichment seems absolutely necessary to coincide with the abundance of experimental evidence. Bolstering the claim of Te segregation is the observation of Te islands on pulsed laser annealed c-CdTe.[36] The incorporation of Te at the GB is based on the previous work of Nelson *et al.*[12] that also showed some degree of Cd and Te segregation prior to PLA treatments. Fig. 4(b) shows that this can be true within our experimental and calculated results if the PLA leads to a larger confinement of the Te-enrichment near GBs (i.e., d becomes smaller to explain Cd:Te ratio increase). Further experimentation is necessary to confirm this.

The analysis presented here is valuable in two respects. First, it shows that a segregation of Te and Cd at the surface of p-CdTe resulting from PLA with Te-enrichment occurring near GBs can explain our experimental results and is consistent with previous observations. Second, this work reveals a possible large source of error when calculating the stoichiometry of multinary material surfaces from XPS data if there is surface segregation. XPS has been used frequently to measure the surface stoichiometry in both p-CdTe and c-CdTe.[30,31,38–44] Specifically, it is often used to investigate

stoichiometry changes induced by a particular surface treatment or processing condition where relative changes are compared to a reference sample.[30,41–44] However, in most cases, even the reference samples give Cd:Te ratios that deviate from the expected stoichiometric value 1:1, which typically goes unexplained. This work shows that the segregation at the surface of even sub-monolayers of Cd and Te leads to large enough deviations from stoichiometry to account for the variations seen in literature (typically about $\pm 10\%$ from stoichiometry). According to our results, variations in surface roughness, which is believed to be a common source of error in XPS quantification, is a smaller effect than segregation. This could be particularly important when XPS is used to study chemical etching effects where the etchants preferentially attack GBs as is often the case for p-CdTe.

Since the model is an approximation of the actual surface morphology, several reasons exist why the values used here could vary from those actually in our samples. First of all, θ is highly dependent on the microscopic geometry of the sample. Therefore, local deviations in θ (not considered here) could have an effect on the angle dependent results, which would especially be true if variations are larger nearer the GB. For instance, if the sidewalls of the grains were not a single slope as assumed in the model but had two characteristic slopes with the larger one nearer the GB, one would anticipate an undersampling of the Te-rich GB region. In addition, assuming distributions of only elemental Te and Cd at the surface excludes the possibility that stoichiometric CdTe also exists at the surface. However, adjusting the model to account for these complexities would not add to the qualitative understanding while only increasing the number of computational variables.

In light of the evidence that PLA causes Te-enrichment at the surfaces of GBs, a picture of the conduction process at the back contact of a photovoltaic device with a PLA pretreatment begins to emerge. Elemental Te is a degenerate p-type semiconductor that lowers the valence band offset at the CdTe surfaces between a Te overlayer and CdTe bulk.[42,43] Thus, a Te overlayer should improve photovoltaic device performance as others have shown.[45,46] However, the additional presence of a Cd overlayer from the PLA treatment further complicates this interpretation. First of all, the solid Cd overlayer assumed in our model is a simplification of what is most likely a slightly Cd-rich CdTe phase. Both interstitial and antisite Cd defects are donors[47] in CdTe making this region increasingly n-type and an impediment to hole conduction through these regions. Kraft *et al.* showed that Cd-rich overlayers produce surface dipoles and thus band offsets that raise the barrier height for hole conduction even when very large work function materials are used.[48] They calculated that a Cd layer as thin as 1/100 of a monolayer was enough to create this effect. Furthermore, several studies have shown that GB cores are depleted of holes and act as efficient minority electron current carrying regions[49–52] while another recent study showed hole conduction at some GBs.[53] A Te-rich region over a hole depleted GB would lead to a non-ohmic junction. In light of our previous work that showed decreased back contact resistance from PLA treated solar cells, it seems that at least some of the GBs must transport holes, although it is certainly possible that both kinds of GB regions exist. Further experimentation is necessary to understand the microscopic nature of current conduction in PLA treated p-CdTe solar cells.

V. CONCLUSIONS

The raw XPS data presented show a Cd-enrichment at the surface of p-CdTe as a result of pulsed UV laser treatment. This is contradictory to the expected result from literature as well as our previous electrical measurements, which all show a Te-enrichment at the surface. To resolve these findings, a model was developed that calculated the effects of surface topology and overlayers on the expected Cd:Te ratio from XPS measurements. These calculations showed that the idea of a uniform Te overlayer at the surface of a pulsed UV treated p-CdTe film was inconsistent with our angle-resolved XPS measurements. By including elemental Te regions localized at the surfaces of grain boundaries and elemental Cd layers at the surface of grain interiors, our XPS results could be explained. It was found that the thicknesses of these Cd overlayers only needed to be on the order of 1 Å to have a significant impact on the Cd:Te ratio whereas varying the surface roughness had only a limited effect. It is only through the inclusion of a Cd overlayer in addition to a Te-rich region at the grain boundary that we find good qualitative agreement with our results that is also consistent with previous literature results.

ACKNOWLEDGMENTS

This work was supported in full by the Department of Energy through the Bay Area Photovoltaic Consortium under Award Number DE-EE0004946. The XPS instrument is part of the University of Utah shared facilities of the Micron Microscopy Suite sponsored by the College of Engineering, Health Sciences Center, Office of the Vice President for Research, and the Utah Science Technology and Research (USTAR) initiative of the State of Utah. We especially thank Professor Ashutosh Tiwari for the generous access to the excimer laser.

[1]*Laser Annealing of Semiconductors*, edited by J. M. Poate and J. W. Mayer (Academic Press, Inc., New York, 1982).
[2]B. J. Simonds, V. Palekis, M. I. Khan, C. S. Ferekides, and M. A. Scarpulla, SPIE Proc. **8826**, 882607 (2013).
[3]B. J. Simonds, V. Palekis, B. Van Devener, C. Ferekides, and M. A. Scarpulla, Appl. Phys. Lett. **104**, 141604 (2014).
[4]Y. Hatanaka, M. Niraula, A. Nakamura, and T. Aoki, Appl. Surf. Sci. **176**, 462–467 (2001).
[5]Y. Hatanaka, M. Niraula, Y. Aoki, T. Aoki, and Y. Nakanishi, Appl. Surf. Sci. **142**, 227 (1999).
[6]M. Niraula, A. Nakamura, T. Aoki, Y. Tomita, and Y. Hatanaka, Phys. Status Solidi **229**, 1103 (2002).
[7]M. Niraula, A. Nakamura, T. Aoki, H. Tatsuoka, and Y. Hatanaka, J. Electron. Mater. **30**, 911 (2001).
[8]P. D. Brewer, J. J. Zinck, and G. L. Olson, Appl. Phys. Lett. **57**, 2526 (1990).
[9]V. A. Gnatyuk, Solid State Phenom. **63–64**, 353 (1998).
[10]L. A. Golovan, P. K. Kashkarov, Y. N. Sosnovskikh, V. Y. Timoshenko, N. G. Chechenin, and V. M. Lakeenkov, Phys. Solid State **40**, 187 (1998).
[11]A. Baidullaeva, A. I. Vlasenko, P. E. Mozol, and A. B. Smirnov, Semiconductors **35**, 745 (2001).
[12]A. J. Nelson, M. Danailov, L. Gregoratti, M. Marsi, and M. Kiskinova, J. Appl. Phys. **87**, 3520 (2000).

[13]L. A. Golovan, B. A. Markov, P. K. Kashkarov, and V. Y. Timoshenko, Solid State Commun. **108**, 707 (1998).
[14]C. S. Ferekides, D. Marinskiy, V. Viswanathan, B. Tetali, V. Palekis, P. Selvaraj, and D. L. Morel, Thin Solid Films **361–362**, 520 (2000).
[15]K. Vutova, G. Mladenov, T. Tanaka, and K. Kawabata, Vacuum **62**, 297 (2001).
[16]K. Vutova, G. Mladenov, T. Tanaka, and K. Kawabata, Surf. Interface Anal. **34**, 597 (2002).
[17]C. S. Fadley, R. J. Baird, W. Siekhaus, T. Novakov, and S. A. L. Bergstroem, J. Electron Spectrosc. Relat. Phenom. **4**, 93 (1974).
[18]R. C. Chatelier, H. A. W. St. John, T. R. Gengenbach, P. Kingshott, and H. J. Griesser, Surf. Interface Anal. **25**, 741 (1997).
[19]K. Olejnik, J. Zemek, and W. S. M. Werner, Surf. Sci. **595**, 212 (2005).
[20]K. Olejnik and J. Zemek, Surf. Sci. **602**, 2581 (2008).
[21]J. Zemek, K. Olejnik, and P. Klapetek, Surf. Sci. **602**, 1440 (2008).
[22]J. Zemek, Anal. Sci. **26**, 177 (2010).
[23]Practival Surface Analysis, edited by D. Briggs and M. P. Seah, 2nd ed. (Wiley, West Sussex, England, 1990).
[24]S. Tougaard, J. Vac. Sci. Technol. A **5**, 1275 (1987).
[25]C. J. Powell, Surf. Sci. **44**, 29 (1974).
[26]C. D. Wagner, L. E. Davis, M. V. Zeller, J. A. Taylor, R. H. Raymond, and L. H. Gale, Surf. Interface Anal. **3**, 211 (1981).
[27]J. H. Scofield, J. Electron Spectrosc. Relat. Phenom. **8**, 129 (1976).
[28]J. F. Moulder, W. F. Stickle, P. E. Sobol, and K. D. Bomben, *Handbook of X-Ray Photoelectron Spectroscopy* (Perkin-Elmer Corp., Eden Prarie, MN, 1992).
[29]T. S. Sun, J. Vac. Sci. Technol. **17**, 1067 (1980).
[30]D. Levi, D. Albin, and D. King, Prog. Photovoltaics **8**, 591 (2000).
[31]D. M. Poirier and J. H. Weaver, Surf. Sci. Spectra **2**, 209 (1993).
[32]V. A. Gnatyuk, T. Aoki, Y. Nakanishi, and Y. Hatanaka, Surf. Sci. **542**, 142 (2003).
[33]T. Aoki, V. A. Gnatyuk, A. Nakamura, Y. Tomita, Y. Hatanaka, and J. Temmyo, Phys. Status Solidi **1**, 1050 (2004).
[34]P. D. Brewer, M. Spath, and M. Stuke, in *Proceedings of the Materials Research Society Symposium* (1994), pp. 245–250.
[35]Y. Yan, M. M. Al-Jassim, K. M. Jones, S.-H. Wei, and S. B. Zhang, Appl. Phys. Lett. **77**, 1461 (2000).
[36]J. J. Zinck, P. D. Brewer, and G. L. Olson, in *Proceedings of the Materials Research Society Symposium* (1991), Vol. **204**, pp. 243–250.
[37]P. W. Allen and L. E. Sutton, Acto Crystallogr. **3**, 46 (1950).
[38]M. D. Stoev, A. P. Katerski, and R. Stefanov, Vacuum **47**, 1231 (1996).
[39]Y.-C. Lu, R. S. Feigelson, and R. K. Route, J. Appl. Phys. **67**, 2583 (1990).
[40]O. Zelaya, J. Vac. Sci. Technol. A **7**, 245 (1989).
[41]A. Waag, Y. S. Wu, R. N. Bicknell-Tassius, and G. Landwehr, Appl. Phys. Lett. **54**, 2662 (1989).
[42]D. W. Niles, X. Li, P. Sheldon, and H. Hoüchst, J. Appl. Phys. **77**, 4489 (1995).
[43]D. Kraft, A. Thissen, J. Broetz, S. Flege, M. Campo, A. Klein, and W. Jaegermann, J. Appl. Phys. **94**, 3589 (2003).
[44]A. J. Ricco, J. Vac. Sci. Technol. A **2**, 910 (1984).
[45]D. W. Niles, X. Li, D. Albin, D. Rose, T. Gessert, and P. Sheldon, Prog. Photovoltaics **4**, 225 (1996).
[46]X. Li, D. W. Niles, F. S. Hasoon, R. J. Matson, and P. Sheldon, J. Vac. Sci. Technol. A **17**, 805 (1999).
[47]S.-H. Wei and S. Zhang, Phys. Rev. B **66**, 155211 (2002).
[48]D. Kraft, U. Weiler, Y. Tomm, A. Thissen, A. Klein, and W. Jaegermann, Thin Solid Films **431–432**, 382 (2003).
[49]I. Visoly-Fisher, S. R. Cohen, A. Ruzin, and D. Cahen, Adv. Mater. **16**, 879 (2004).
[50]I. Visoly-Fisher, S. R. Cohen, K. Gartsman, A. Ruzin, and D. Cahen, Adv. Funct. Mater. **16**, 649 (2006).
[51]S. Smith, P. Zhang, T. Gessert, and A. Mascarenhas, Appl. Phys. Lett. **85**, 3854 (2004).
[52]P. Sutter, E. Sutter, and T. R. Ohno, Appl. Phys. Lett. **84**, 2100 (2004).
[53]K. Alberi, B. Fluegel, H. Moutinho, R. G. Dhere, J. V. Li, and A. Mascarenhas, Nat. Commun. **4**, 2699 (2013).